Cell Structure and Global Heat Release in 2D and 3D JP10-Air Detonations in Narrow Channels

Patrick A. Meagher[1], Xian Shi[2], Xinyu Zhao[1],
Sai Sandeep Dammati[3], Alexei Y. Poludnenko[1,3], Hai Wang[2]

[1]Department of Mechanical Engineering, University of Connecticut, Storrs, CT, USA
[2]Department of Mechanical Engineering, Stanford University, Stanford, CA, USA
[3]Department of Aerospace Engineering, Texas A&M University, College Station, TX, USA

1 Introduction

Detonation for energy conversion applications presents potentially significant improvements in terms of both efficiency and performance [1]. While significant efforts have been made in detonation simulations using detailed reaction kinetics, most studies have been conducted for detonations of hydrogen or small hydrocarbons [2–6]. Very little attention has been placed on liquid hydrocarbon fuels, even though liquid-fueled detonations present a number of advantages in practical propulsion systems [7]. Multi-phase detonation studies are available for flows comprising of liquid fuel droplets and gaseous oxidizer using simplified chemical kinetic models [7, 8]. To the authors' knowledge, only one prior study employed detailed chemical kinetics model to describe both pyrolysis and oxidation processes in jet fuel detonations, however this study was limited to two-dimensional (2D) simulations on relatively coarse computational grids [9]. The present study aims to expand our understanding of detonations in a real jet fuel, JP10 ($C_{10}H_{16}$) through 2D and three-dimensional (3D) Navier-Stokes simulations with realistic boundary conditions and a detailed chemical kinetic model. An emphasis of our study is the relationship between the detonation cellular structure and global characteristics of the heat release.

2 Numerical Methods

The compressible Navier-Stokes equations are solved on the fixed uniform grid with a massively parallel code `Athena-RFX` [10,11], a reactive-flow extension of the magnetohydrodynamics code `Athena` [12]. Convective fluxes are calculated with the HLLC-ADC (Anti-Diffusion Control) scheme to minimize carbuncles [13], and flow integration is performed with a second-order accurate Godunov scheme employing the unsplit corner transport upwind (CTU) method [14]. A piecewise linear method (PLM) [15] is used for state reconstruction. Net diffusive fluxes are calculated with a second-order finite difference method with flux matching to maintain conservation [10]. Flow and chemistry are coupled through Strang splitting [16] with a global reaction-advection time-step control. This methodology is of second-order accuracy in both time and space.

Pyrolysis and oxidation reactions of JP10 combustion are modeled using the skeletal version of the HyChem model for JP10 [17]. Chemical source terms are integrated using the non-iterative, single-step, semi-implicit ODE integrator YASS [18].

3   Computational Configuration

For this study, both 2D and 3D simulations are conducted in the laboratory reference frame, with cellular detonations propagating into a quiescent stoichiometric JP10/air mixture at 5 bar and 600 K. According to steady-state 1D detonation calculations performed using the Shock and Detonation Toolbox [19], at these mixture conditions, the CJ speed D_{CJ} is 1.81 km/s, the ZND induction length Δ_i is 491 μm, and the ZND exothermic pulse width Δ_e is 93.7 μm. The 2D computational domain is 4.92 cm in the streamwise direction and 1.98 cm in the spanwise direction. The 3D domain is a square duct of length 4.92 cm in the streamwise direction and 1.98 cm in the spanwise and transverse directions. In terms of normalized dimensions, the computational domain is approximately $100\Delta_i \times 40\Delta_i$ in 2D and $100\Delta_i \times 40\Delta_i \times 40\Delta_i$ in 3D. The detonation structure is resolved using 26 computational cells per Δ_i, or 5 cells per Δ_e. This resolution is a compromise between accuracy and feasibility of the 3D simulation, with the 3D grid consisting of approximately 2.9 billion computational cells. The current 3D computation has consumed approximately 10 million CPU hours on 256 AMD EPYC 7H12 processors. The 2D simulation time is 2.72×10^{-4} s, which corresponds to $\approx 1000\Delta_i$ of propagation distance, while the 3D simulation was followed for 7.57×10^{-5} s, or $\approx 280\Delta_i$ of propagation.

In all cases, the upstream boundary condition is zero-gradient and downstream boundary is specified by the CJ state. All side walls are isothermal, no-slip with a wall temperature of 600 K. Detonations are initialized with a spatially perturbed sinusoidal ZND profile calculated using the Shock and Detonation Toolbox [19]. This approach produces rapid cellular instabilities and minimizes the initial transient period. To minimize the domain length, a moving grid technique is employed, which shifts the solution downstream and introduces fresh quiescent gas upstream at discrete intervals.

4   Results and Discussion

4.1   Global Heat Release and Cellular Structure in 2D

To quantify the effect of wall losses on the global burning rate, the mean heat release rate (HRR) is calculated as

$$Q = \frac{1}{L_y}\frac{1}{L_z}\int_0^{L_x}\int_0^{L_y}\int_0^{L_z}\dot{q}(x,y,z)\mathrm{d}x\mathrm{d}y\mathrm{d}z,$$

where $\dot{q}(x,y,z)$ is the local volumetric HRR, and L_x, L_y, and L_z are the domain length in the streamwise direction and the two spanwise directions respectively. In 2D, $\dot{q}$ is a function of x and y only. The above burning rate can be normalized by the HRR for the CJ detonation, $Q_{CJ} = \rho_0 D_{CJ}\Delta Q$, where ρ_0 is the density of the unburnt gas, D_{CJ} is the CJ detonation speed, and ΔQ is the difference in the chemical enthalpy between the unburnt and burnt CJ state per unit mass. The quantity Q/Q_{CJ} allows for the comparison of the temporally evolving burning rate from the multidimensional simulations to that of a CJ detonation, with $Q/Q_{CJ} < 1$ indicating the burning rate to be insufficient to maintain a detonation at the CJ speed. In contrast, $Q/Q_{CJ} > 1$ indicates that global burning is in excess of the CJ.

Figure 1 shows the numerical soot foil and the HRR in the 2D simulation. It can be seen that $Q/Q_{CJ} < 1$ fluctuates around unity with an average $Q/Q_{CJ} = 1.02$. Hence, the impact of wall losses appears to be small, and the total power is close to that of a CJ detonation. Appreciable fluctuations are however observed in Q/Q_{CJ} with a standard deviation of $0.16Q_{CJ}$. This fluctuation was analyzed for its power spectral density (PSD) using Welch's method [20, 21] and plotted in Fig 1(b). A single dominant period is seen at 22 μs or 46 kHz. Estimating the detonation wave speed as that of the CJ detonation, this frequency correlates to a length scale of 4 cm. Examining the soot foil in Fig. 1(c), we found the above 4 cm length scale to be significantly longer than the typical detonation cell length.
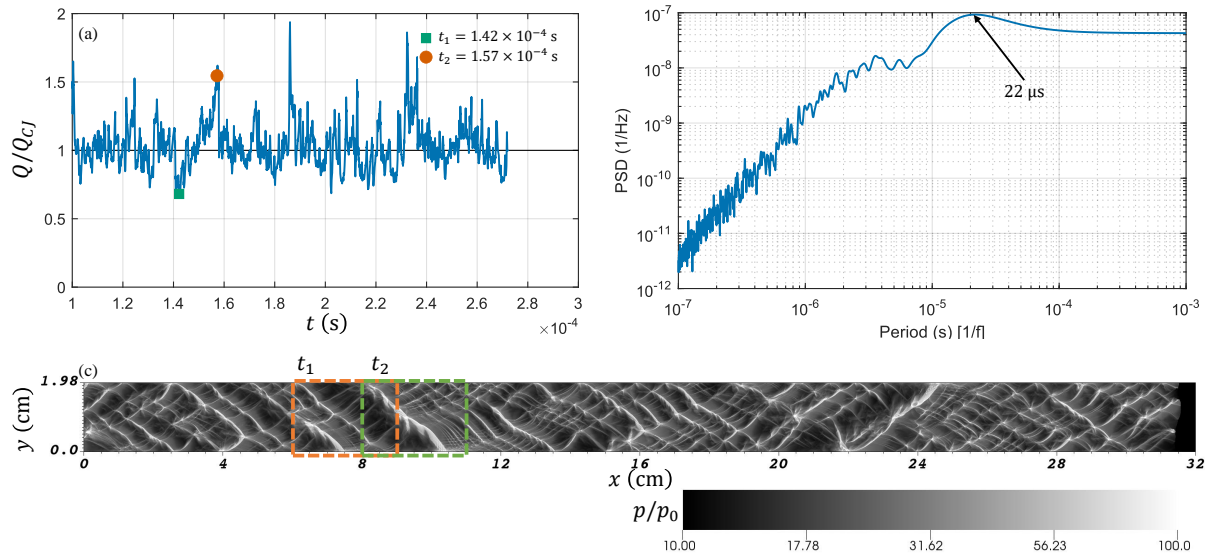
Figure 1: Key results from a 2D simulation of JP10-air detonation at 5 bar and 600 K. (a) Normalized global heat release rate as a function of time. (b) Power spectral density of the normalized global heat release rate. (c) Numerical soot foil showing the maximum normalized pressure p/p_0 for the temporal window shown in (a). The detonation propagates from left to right. See text for the explanation of the two points in panel (a) and the two boxes in panel (c).
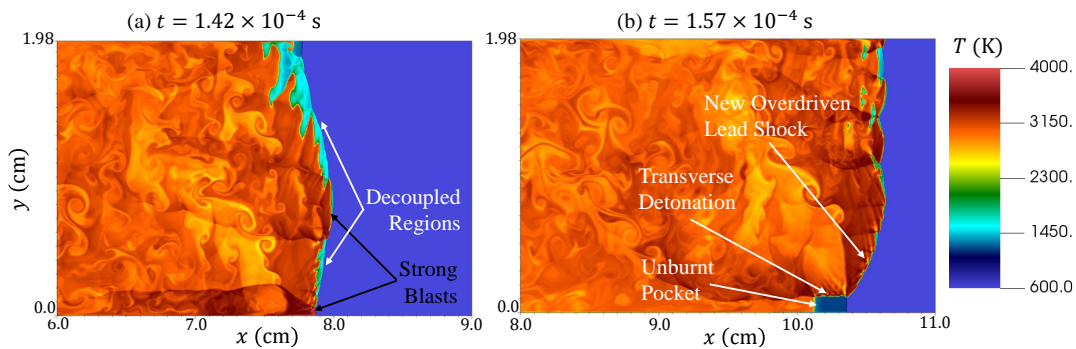
Figure 2: Instantaneous temperature fields at (a) $t = 1.42 \times 10^{-4}$ and (b) $t = 1.57 \times 10^{-4}$ s, computed for the JP10-air detonation at 5 bar and 600 K. Detonation propagates from left to right, and x-coordinate coincides with the boxes marked in the numerical soot foil in Fig. 1.

To further investigate the variation in global burning, temperature fields at two instances, $t_1 = 1.42 \times 10^{-4}$ and $t_2 = 1.57 \times 10^{-4}$ (see Fig. 1a), are extracted from the simulation and shown in Fig 2. At t_1, a minimum in the burning rate is observed, with $Q/Q_{CJ} = 0.68$. At t_2, however, the heat release reaches a local maximum with $Q/Q_{CJ} = 1.55$. The period of detonation wave evolution is particularly interesting. At t_1, the soot foil shows that the number of the triple point traces has greatly decreased, and the remaining triple points are weakened, as indicated by the dark gray (lower maximum pressure) rather than bright white (higher maximum pressure) regions. From the instantaneous temperature field, we find that the detonation in the upper half of the domain and most of the lower half has essentially degraded into a decoupled shock and trailing reaction waves. Only two strongly coupled waves are present, one in the center of the domain and one at the lower wall.

As the detonation front evolves, the reaction wave falls further behind the shock wave in these decoupled
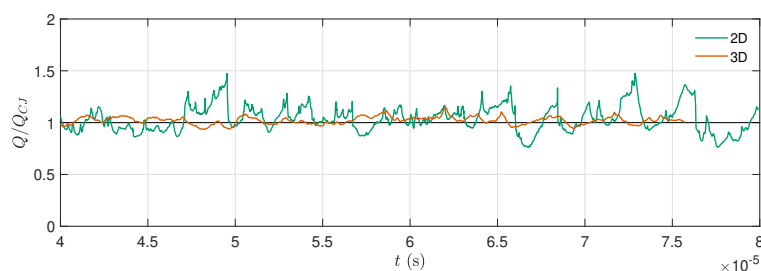
Figure 3: Normalized global heat release rate for 2D (green) and 3D (orange) simulations of JP10-air detonation at 5 bar and 600 K.

regions, producing large volumes of shock-heated but unburnt reactants. These decoupled regions are typically consumed by transverse detonations waves at a later time, and they leave wide, bright traces on the soot foil, much broader than typical triple point traces. One such trace starts at the upper wall at $x = 8$ cm and travels diagonally downward, terminating at $x = 10.5$ cm on the lower wall. The final stages of this transverse detonation are captured in Fig. 2(b), where a 0.25 cm wide pocket of shock heated but unburnt mixture can be observed at the lower wall. A nearly horizontal detonation front is proceeding downward, as is evident from the clear discontinuity in temperature. This transverse detonation increases the global burning rate through two mechanisms. First, the volumetric heat release rate in the transverse detonation is 80 times the peak value from the ZND solution due to a combined effect of the increased density and temperature of the unburnt fuel pocket. Second, the transverse detonation produces a new overdriven shock, as can be seen by the dark red region upstream of the transverse detonation. The combination of rapid burning in the unburnt pocket and the newly formed overdriven shock leads to a significant increase in global burning rate at t_2.

As the detonation evolves from the quasi-failure at t_1 to the transverse detonation propagation at t_2, Q/Q_{CJ} crosses unity (cf. Fig. 1). The time between individual instances when $Q/Q_{CJ} = 1$ is $\approx 17 \mu$s, which is similar to the dominant 22 μs period from the spectral analysis. This, coupled with knowledge that the associated length scale is much greater than the characteristic cell length, suggests that the global burning in the unstable 2D detonation described here is governed primarily by the interactions between multiple detonation cells and associated transverse waves, rather than by the individual detonation cells.

4.2 Findings from Preliminary 3D Simulations

Figure 3 shows the comparison of the normalized HRR in the 2D and 3D simulations. After the initial transient ($t < 4 \times 10^{-5}$ s, not shown here), both 2D and 3D simulations relax to a quasi-steady cellular propagation. Detonation in 3D is decidedly more stable than in 2D. The global HRR is much steadier in 3D than in 2D (Fig 3). The standard deviation in Q/Q_{CJ} is 3.6% in 3D, while it is 15% in 2D. The stabilizing effect is also apparent in Fig 4, where no evidence of large-scale decoupling and transverse detonation formation seen in the 2D simulation is present in 3D.

5 Concluding Remarks

Results are presented from 2D and preliminary 3D simulations of cellular detonations in JP10 employing the Navier-Stokes equations and the detailed chemical kinetic model. Global burning rate is quantified and compared to that of a CJ detonation. In 2D, global burning rate was found to be highly oscillatory, with an instantaneous burning rate ranging from 70% to over 150% of that in the CJ detonation. The dominant frequency for the global burning rate is approximately 46 kHz, equivalent to a period of 22 μs
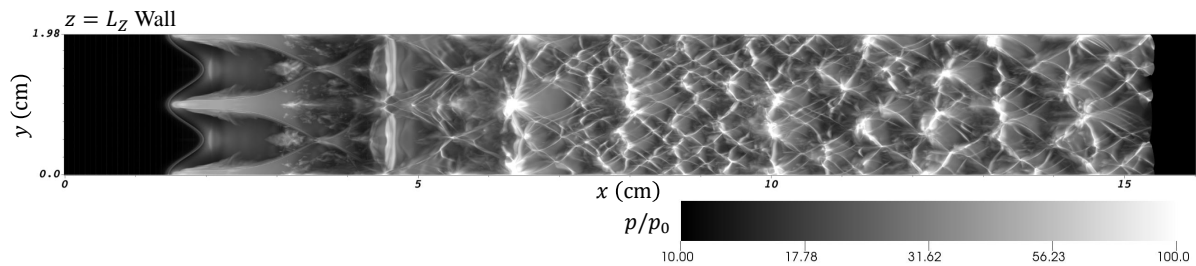
Figure 4: Maximum-pressure-based numerical soot foils from the simulation of a JP10-air detonation at 5 bar and 600 K, captured along the $z = L_z$ exterior wall. The detonation propagates from left to right.

or wavelength of 4.0 cm. This length scale is significantly longer than the characteristic detonation cell size. The evolution from a local minimum to a local maximum in 2D burning rates is explained through the decoupling of a shock and a trailing reaction front followed by transverse detonation formation, where a detonation wave sweeps through the shock-heated but unburnt gas. The timescale of this sequence is similar to the dominant period identified in the spectral analysis. Preliminary results suggest that in 3D the decoupling and transverse detonations are less prevalent, which results in a substantially smaller variation in the global burning rate than in 2D. Furthermore, evidence of the decoupling and transverse detonation mechanism is absent on the 3D soot foil. Finally, we note that the 3D results are preliminary, and as the 3D simulation progresses, it is possible that the quasi-failures and re-ignition events may develop.

Acknowledgements

References

[1] P. Wolański, "Detonative propulsion," *Proceedings of the Combustion Institute*, vol. 34, pp. 125–158, 2013.

[2] B. Taylor, D. Kessler, V. Gamezo, and E. Oran, "Numerical simulations of hydrogen detonations with detailed chemical kinetics," *Proceedings of the Combustion Institute*, vol. 34, no. 2, pp. 2009–2016, 2013.

[3] K. Eto, N. Tsuboi, and A. K. Hayashi, "Numerical study on three-dimensional CJ detonation waves: detailed propagating mechanism and existence of OH radical," *Proceedings of the Combustion Institute*, vol. 30, no. 2, pp. 1907–1913, 2005.

[4] N. Tsuboi, Y. Daimon, and A. K. Hayashi, "Three-dimensional numerical simulation of detonations in coaxial tubes," *Shock Waves*, vol. 18, no. 5, pp. 379–392, 2008.

[5] X. Cai, J. Liang, Z. Lin, R. Deiterding, and Y. Liu, "Parametric study of detonation initiation using a hot jet in supersonic combustible mixtures," *Aerospace Science and Technology*, vol. 39, pp. 442–455, 2014.

[6] T. Araki, K. Yoshida, Y. Morii, N. Tsuboi, and A. K. Hayashi, "Numerical analyses on ethylene/oxygen detonation with multistep chemical reaction mechanisms: Grid resolution and chemical reaction model," *Combustion Science and Technology*, vol. 188, no. 3, pp. 346–369, 2015.

[7] D. A. Schwer, "Multi-dimensional simulations of liquid-fueled JP10/oxygen detonations," in *AIAA Propulsion and Energy 2019 Forum*, American Institute of Aeronautics and Astronautics, Aug. 2019.

[8] A. K. Hayashi, N. Tsuboi, and E. Dzieminska, "Numerical study on JP-10/air detonation and rotating detonation engine," *AIAA Journal*, vol. 58, no. 12, pp. 5078–5094, 2020.

[9] L. Liu and Q. Zhang, "Numerical study of cellular structure in detonation of a stoichiometric mixture of vapor JP-10 in air using a quasi-detailed chemical kinetic model," *Aerospace Science and Technology*, vol. 91, pp. 669–678, 2019.

[10] A. Poludnenko and E. Oran, "The interaction of high-speed turbulence with flames: Global properties and internal flame structure," *Combustion and Flame*, vol. 157, no. 5, pp. 995 – 1011, 2010.

[11] Y. Kozak, S. Dammati, L. Bravo, P. Hamlington, and A. Poludnenko, "WENO interpolation for Lagrangian particles in highly compressible flow regimes," *Journal of Computational Physics*, vol. 402, p. 109054, 2020.

[12] J. M. Stone, T. A. Gardiner, P. Teuben, J. F. Hawley, and J. B. Simon, "Athena: A new code for astrophysical MHD," *Astrophys. J. Supp.*, vol. 178, no. 1, pp. 137–177, 2008.

[13] S. Simon and J. Mandal, "A cure for numerical shock instability in HLLC Riemann solver using antidiffusion control," *Computers & Fluids*, vol. 174, pp. 144 – 166, 2018.

[14] T. A. Gardiner and J. M. Stone, "An unsplit Godunov method for ideal MHD via constrained transport in three dimensions," *J. Comp. Phys.*, vol. 227, no. 8, pp. 4123 – 4141, 2008.

[15] E. F. Toro, *Riemann Solvers and Numerical Methods for Fluid Dynamics: A Practical Introduction.* Springer Science & Business Media, 2013.

[16] G. Strang, "On the construction and comparison of difference schemes," *SIAM Journal on Numerical Analysis*, vol. 5, no. 3, pp. 506–517, 1968.

[17] Y. Tao, R. Xu, K. Wang, J. Shao, S. E. Johnson, A. Movaghar, X. Han, J.-W. Park, T. Lu, K. Brezinsky, F. N. Egolfopoulos, D. F. Davidson, R. K. Hanson, C. T. Bowman, and H. Wang, "A Physics-based approach to modeling real-fuel combustion chemistry – III. Reaction kinetic model of JP10," *Combustion and Flame*, vol. 198, pp. 466–476, 2018.

[18] A. Khokhlov, "YASS-yet another stiff solver that works," Technical Memorandum Report, Naval Research Laboratory, 1999.

[19] Shock and Detonation Toolbox - 2021 Version, Explosion Dynamics Laboratory, California Institue of Technology, https://shepherd.caltech.edu/EDL/PublicResources/sdt/, 2021.

[20] M. H. Hayes, *Statistical digital signal processing and modeling.* New York: John Wiley & Sons, 1996.

[21] P. Stoica, *Spectral analysis of signals.* Upper Saddle River, N.J: Pearson/Prentice Hall, 2005.